

A NUMERICAL PROCEDURE FOR SIMULATION OF HYDRAULICALLY-DRIVEN FRACTURE PROPAGATION IN POROELASTIC MEDIA

THOMAS J. BOONE AND ANTHONY. R. INGRAFFEA

*Program of Computer Graphics, and School of Civil and Environmental Engineering,
Cornell University, Ithaca, NY 14853-3501, U.S.A.*

SUMMARY

A procedure for numerical approximation to two-dimensional, hydraulically-driven fracture propagation in a poroelastic material is described. The method uses a partitioned solution procedure to solve a finite element approximation to problems described by the theory of poroelasticity, in conjunction with a finite difference approximation for modelling fluid flow along the fracture. An equilibrium fracture model based on a generalized, Dugdale–Barenblatt concept is used to determine the fracture dimensions. An important feature is that the fracture length is a natural product of the solution algorithm. Two example problems verify the accuracy of the numerical procedure and a third example illustrates a fully-coupled simulation of fracture propagation. Photographs taken from a high-performance engineering workstation provide insight into the nature of the coupling among the physical phenomena.

INTRODUCTION

Hydraulic fracturing is a method commonly used in the oil industry for enhancing the production of hydrocarbons from wells. There have been numerous numerical methods developed for the simulation of this process.^{1,2} Most of these methods assume that the rock mass is a solid, elastic continuum. The resultant formulation requires the solution of an approximation to two distinct but coupled physical phenomena: elastic deformation of the rock mass and fluid flow in the fracture. Often, fluid loss from the fracture into the rock mass is accommodated by a simple one-dimensional model. However, this approach ignores any effects associated with the coupled processes such as changes in the deformation due to diffusion of the pore pressure or flows and pressures induced by mechanical deformation. The numerical scheme presented in this paper differs from other schemes by assuming the rock mass to be a fully coupled, poroelastic medium. This approximation introduces a third physical phenomenon which is fluid flow in the rock mass.

The physical problem is represented schematically in Figure 1. A vertical borehole extends through the rock mass. The borehole has been hydraulically pressurized until a fracture has initiated and is seen propagating through the rock mass. Several features which are illustrated in Figure 1 are incorporated in the numerical procedure that is described herein. First, the crack-tip is seen to close smoothly, which is a distinctive feature of the non-linear, Dugdale–Barenblatt fracture mechanics model. Secondly, there is coupling between the fluid flow in the fracture and in the rock mass. Finally, the flow along the fracture does not necessarily reach the fracture tip, so a region may exist near the crack-tip which is void of fluid.

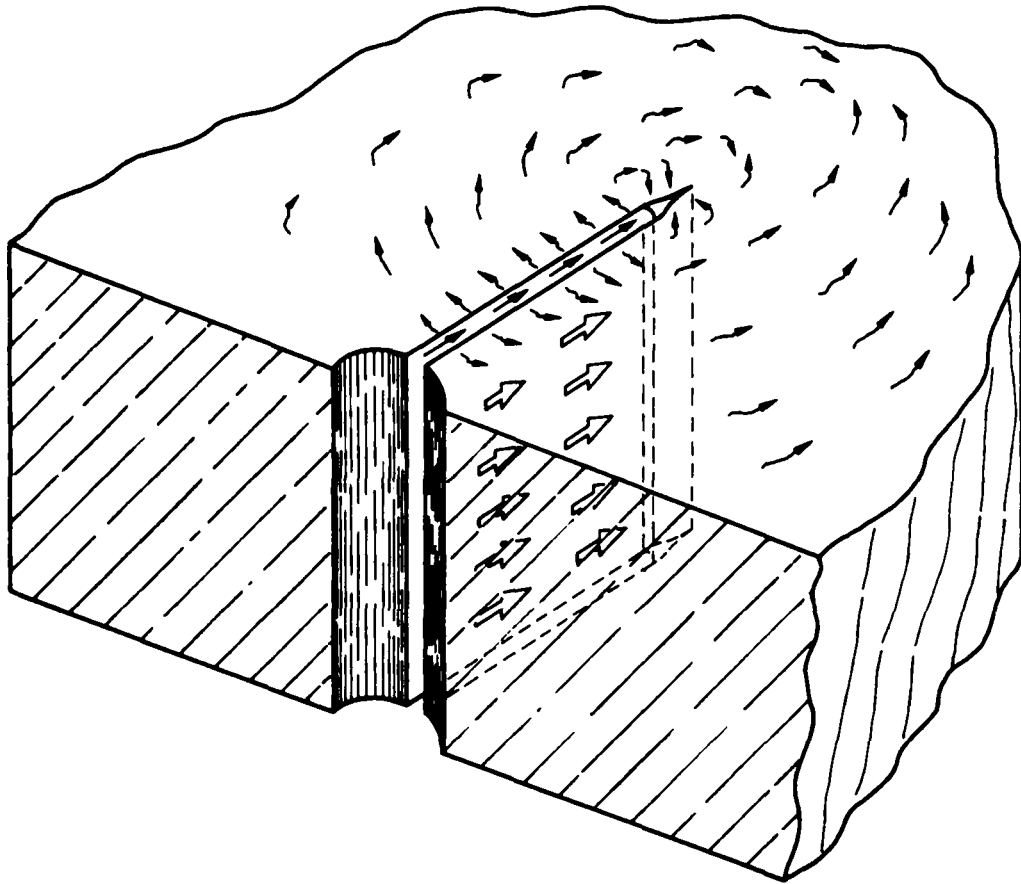


Figure 1. A schematic illustration of a hydraulically driven fracture in a poroelastic medium

Numerical approximation of coupled problems

Coupled problems include a diverse and extensive range of physical phenomena³ as well as presenting some unique challenges for numerical approximation. These challenges have been discussed in detail by Park and Fillipa^{4,5} and Zienkiewicz.⁶ In general, each of the coupled physical phenomena is represented by a governing differential equation and a numerical approximation to that equation. Commonly, the coupling involves a time-dependent process. The numerical approximations to the phenomena may combine a variety of methods such as finite elements, boundary elements or finite differences. The solution procedure described herein uses the finite element method to approximate the deformation of, and the fluid flow within, the rock mass, and a finite difference approximation for the fluid flow along the fracture.

Coupling can also be classified as boundary coupling, as is the case for the coupling between the fluid flow in the fracture and the poroelastic rock mass, or domain coupling as is the case for the mechanical deformation and fluid flow within a poroelastic media. This distinction can have a significant influence on the solution procedures that are employed.

Two fundamentally distinct numerical procedures can be applied to the solution of sets of coupled equations.⁴ The traditional, and most straightforward is to assemble the various approximations in a single composite set of equations and attempt to solve the complete set.

Alternatively, a partitioned solution procedure involves solution of the numerical approximations separately. Explicit, implicit or combined methods can be used to advance the solutions through time. In an explicit, time-marching scheme, information is exchanged between the individual solvers once at the end of the current time step and then each individual solver advances its respective fields or variables. For an implicit scheme, it is usually necessary to iterate at each time step. The separate solvers can then exchange information at each step of the iteration, until an acceptable solution to the coupled sets of equations is found. A partitioned analysis procedure is the method generally favoured.^{4,6} The advantages of a partitioned approach are as follows:

1. Well-proven procedures, which have been developed for uncoupled problems and which are particularly applicable to the specific set of equations, can be employed.
2. The resulting computer code is modular so that alternative solution methods that may include different physical approximations, or improved algorithms can easily be interchanged or included as analysis options.
3. By using computationally efficient solvers for the individual sets of equations, overall efficiency can be attained.
4. As noted by Zienkiewicz,⁶ use of partitioned solvers allows one to develop insight into the strength of coupling between equations.
5. Finally, the open structure of the solution procedure allows incorporation of adaptive control features that can be used to restrict the range of the solution (i.e. to a physically realistic range for a given response) during the iterative process.

The primary disadvantage of partitioned solvers is that one normally cannot determine explicitly convergence and stability requirements for either time-marching or iterative procedures. Generally, the stability requirement for each of the individual methods can be determined. However, this does not guarantee stability of the overall scheme. Typically, the limits of overall stability are determined through trial and error.

Application of the theory of poroelasticity to fracture propagation

The basic linear theory of poroelasticity was first formulated by Biot⁷ in 1941. Since then, Biot⁸ and others such as Rice and Cleary⁹ have made significant contributions to its development. Specifically, the work of Rice and Cleary has given greater physical significance to Biot's work. The theory is commonly applied to soil mechanics problems, especially those involving liquefaction or consolidation.

There is a limited amount of work that investigates fracture in poroelastic materials. Poroelastic effects on fracture propagation have been discussed by Cleary.^{10,11} Cleary and others have performed a numerical investigation where some poroelastic effects were quantified in terms of a stress which acted to resist the crack-opening. Analytical solutions for semi-infinite fractures propagating in poroelastic media have been presented by Ruina¹² and Huang and Russell.^{13,14} Ruina has shown that the apparent material resistance to fracture propagation, or apparent fracture toughness (K_q), increases with the fracture velocity. Ruina's solution is applicable to a hydraulically-loaded fracture propagating at a constant rate with impermeable crack faces. Huang and Russell's work extends these results to hydraulically-loaded fractures propagating at a constant velocity where the fracture walls are permeable. The authors have discussed these effects in more detail in Reference 15. It can be concluded from these works that poroelasticity can have the following significant effects on hydraulically driven fractures: (1) there can be time-dependent changes in the stiffness of the structure due to differences between drained and undrained material properties, (2) diffusion of the pore pressure can alter the mechanical deformations and (3) there

can be a velocity-dependent change in the apparent fracture toughness of the material if a failure criterion based on the (Terzaghi) effective stress is applicable.

In the following section, the equations assumed to govern these phenomena are reviewed. Numerical approximations to the equations are then presented and the integration of the approximations is described. Three example problems illustrate verification of the procedure and some of its capabilities. Finally, the unique features and the limitations of procedure are discussed along with the significance of the examples.

GOVERNING EQUATIONS

Theory of linear poroelasticity

Five material constants are required to define a poroelastic system. Typically, these are G , the drained shear modulus, ν the drained Poisson's ratio, ν_u the undrained Poisson's ratio, B , Skempton's pore pressure coefficient and k , the intrinsic permeability which has dimensions of length squared (Darcies). These parameters can readily be determined experimentally. Rice and Cleary⁹ have show how these parameters relate to micromechanical ones which include ϕ , the porosity, K_f , the bulk modulus of the fluid, K_s , the bulk modulus of the solid grains, and K , the bulk modulus of the porous, solid skeleton, as well as ν and k .*

The governing equations in the absence of body forces and fluid sources can be written as¹⁶

Constitutive relations

$$\sigma_{ij} + \alpha p \delta_{ij} = 2G e_{ij} + \frac{2G\nu}{1-2\nu} \delta_{ij} e \quad (1)$$

$$p = -\frac{2GB(1+\nu_u)}{3(1-2\nu_u)} e + \frac{2GB^2(1-2\nu)(1+\nu_u)^2}{9(\nu_u-\nu)(1-2\nu_u)} \zeta \quad (2)$$

Equilibrium equations

$$\sigma_{ij,j} = 0 \quad (3)$$

Darcy's law

$$q_i = \kappa p_{,i} \quad (4)$$

Continuity equation

$$\frac{\delta \zeta}{\delta t} + q_{i,i} = 0 \quad (5)$$

where σ_{ij} is the total stress, e_{ij} is the strain, ζ is the variation of the fluid content per reference volume, q_i is the specific discharge vector, κ is the permeability coefficient equivalent to k/μ , μ is the fluid viscosity, and δ_{ij} is the Kronecker delta. The poroelastic constant, α , is independent of the fluid properties, and is defined as

$$\alpha = \frac{3(\nu_u - \nu)}{B(1-2\nu)(1+\nu_u)} = 1 - \frac{K}{K_s} \quad (6)$$

* Rice and Cleary introduce three physical constants, K_s , K'_s and K''_s in place of simply K_s . In the special case where all fluid is contained in interconnected pore space, it can be assumed that $K_s = K'_s = K''_s$.

By definition, the total stress is related to the effective stress (assuming that tension is positive) as follows:

$$\sigma_{ij} = \sigma'_{ij} - p \quad (7)$$

where σ'_{ij} is the Terzaghi effective stress, which is assumed to govern failure of the material.¹⁷

Fluid flow along the fracture

The simplest appropriate model for flow in a fracture is embodied in lubrication theory.¹⁸ It assumes that the flow is laminar, the fluid is incompressible, and accounts for the time-dependent rate of crack opening. It can be stated as follows:

$$\frac{\delta q}{\delta x} - \frac{\delta w}{\delta t} + q_1 = 0 \quad (8)$$

$$q = -\frac{w^3}{12\mu} \frac{\delta p}{\delta x} \quad (9)$$

where q is the flow along the fracture length x , q_1 is the fluid loss into the rock mass, μ is the viscosity of the fluid in the fracture, p is the pressure in the fracture and w is the crack opening.

NUMERICAL APPROXIMATIONS

Finite element approximation to the theory of poroelasticity

The theory of poroelasticity can be approximated using the finite element method and a Galerkin formulation, as described by Zienkiewicz.¹⁹ It is applied commonly to soils. An important distinction when applying the formulation to rock is that the compressibility of the constitutive materials must be considered. Typically, for soils B and α are both assumed to equal one whereas for rock these values may be significantly less than one.⁹ The finite element equations, in matrix notation, are as follows:

$$[\mathbf{K}]\{\mathbf{u}\} + [\mathbf{L}]\{\mathbf{p}\} = \{\mathbf{f}\} \quad (10)$$

$$[\mathbf{S}]\{\dot{\mathbf{p}}\} + [\mathbf{L}]^T\{\dot{\mathbf{u}}\} + [\mathbf{H}]\{\mathbf{p}\} = \{\mathbf{q}\} \quad (11)$$

Here \mathbf{u} are the nodal displacements, \mathbf{p} the nodal pressures, \mathbf{f} the nodal loads, \mathbf{q} the nodal flows, $[\mathbf{K}]$ the stiffness matrix, $[\mathbf{L}]$ the coupling matrix, and $[\mathbf{H}]$ the flow matrix. The matrices are fully defined in the Appendix. Equation (10) is known as the stiffness equation and equation (11) is the flow equation.

Three-sided and four-sided isoparametric elements with quadratic displacement fields and linear pore-pressure fields are used in the example problems. Sandu, Liu and Singh²⁰ have shown that there is little advantage to employing a quadratic pore pressure approximation across elements. Along the fracture path, six-noded, zero-thickness, interface elements are inserted into the finite element mesh.²¹ These elements provide the conduit for flow along the fracture and also serve to model the non-linear fracture process zone which is described in the next section. Initially, they are assigned a nominal elastic stiffness that is large enough not to allow any significant overlap or opening along the crack path.

Fracture mechanics model

A non-linear, generalized Dugdale–Barenblatt, fracture mechanics model²² can be incorporated into the zero-thickness interface elements. This model is described in detail in Reference²³. For the purposes of this paper it is assumed that the rock has a negligible fracture toughness (K_{Ic}) or fracture energy (G_{Ic}). In some circumstances, this is an appropriate assumption for hydraulic fracturing.²⁴ However, it is not meant to imply that fracture mechanics is unimportant. It is still necessary to determine a fracture length where the fracture is in equilibrium between the *in situ* stress and the pressure distribution in the fracture.

The method used here requires that the crack path be predetermined. The interface elements, which have been inserted along the path, prevent the fracture from closing past the point where the fracture faces would be in contact, and allow the fracture to open when subjected to tensile stress or internal pressurization. In general, an iterative procedure must be used to solve for the length and opening of the crack.

An important feature of the method is that the fracture length is a natural product of the solution procedure. Other researchers have employed methods that required discrete increments of the fracture length followed by updating of the fluid flow equations.²⁵ The method used here is advantageous since it naturally accommodates either a progressing or a receding fracture which can result from variations in the flow rate at the crack-mouth. It may have even more significant advantages in three dimensions, where a crack-front moves, rather than a crack-tip, so that incrementing the crack's dimensions becomes a more complex process.

Advantages and limitations of the finite element approach

When employing the finite element method as described above, one must be acutely aware of the interrelationship between finite element dimensions and time scales. It is appropriate here to introduce a non-dimensional time scale τ , where $\tau = ct/L^2$.²⁶ The diffusivity coefficient, c , is defined as

$$c = \frac{2GB^2\kappa(1-\nu)(1+\nu_u)^2}{9(\nu_u-\nu)(1-\nu_u)} \quad (12)$$

and L is a characteristic length. To model short periods of time accurately, the finite element dimensions must be sufficient to resolve the pore pressure gradients. For an element with length of L_e , on a boundary subjected to a sudden change in the boundary conditions, time periods greater than approximately L_e^2/c are modelled reasonably accurately. Elements away from the boundary are generally not subjected to the same magnitudes of pore pressure gradient and can be sized accordingly.

A significant difference between elasticity and poroelasticity is that far-field boundary conditions may significantly affect local displacements. This effect is related to the pore pressure field which can geometrically diverge. However, for a mesh spanning a total dimension of L_T , the local displacements and pressures are largely independent of the far field, pore pressure and flux boundary conditions for a time period of only L_T^2/c . These length-scale considerations can largely be overcome through the use of a boundary element formulation^{27,28} or by employing specially developed finite elements.^{29,30} The finite element method has advantages when considering non-linear material parameters such as stress or thermally dependent poroelastic properties, a non-Darcy flow model in the rock or layered rock masses. These models are more readily incorporated into a finite element method. Clearly, parallel development of both finite and boundary element methods is desirable.

Finite difference model of flow along a fracture

A control-volume approach has been devised to model the fluid flow in the fracture. It is illustrated in Figure 2 and can be written in the following form where subscripts represent spatial nodes and superscripts represent time steps:

$$-q_{i-1/2}^{t+1} + q_{i+1/2}^{t+1} + \frac{w_i^{t+1} - w_i^t}{\Delta t} \Delta x - q_{ii}^{t+1} = 0 \quad (13)$$

$$q_{i+1/2}^{t+1} = \frac{w_{i+1/2}^{t+1}^3}{12\mu} \frac{p_i^{t+1} - p_{i-1}^{t+1}}{\Delta x} \quad (14)$$

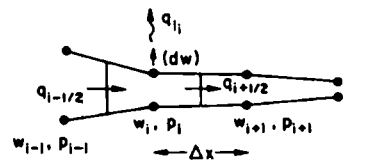
The crack opening, w , is obtained from the finite element equations so that the unknown in the equations above is the pressure, p^{t+1} . Assembly of the equations for the individual control volumes results in a tridiagonal matrix.

This model for the fluid flow is initially constructed for the complete length of the predetermined fracture path. The control volumes are given a nominal, small initial width so that the equations are well-posed. The boundary conditions for each time step are specified as a fixed pressure at the crack mouth and zero flow at the other end of the fracture. The fracturing fluid is assumed to be incompressible so that there can be no flow past the tip of the fracture, even though the zero-flow condition is imposed at the end of the row of control volumes.

An imposed flow as a boundary condition for the crack mouth is a desirable alternative. In order to impose this boundary condition, in conjunction with the partitioned analysis procedure used here, it would be necessary to impose a pressure boundary condition elsewhere along the fracture. Generally, the pressure along the fracture is not known and it cannot be imposed at the crack-tip owing to the existence of a singularity in the pressure at this point.³¹

Integration of the numerical approximations

The finite element approach naturally integrates the fluid flow in the rock mass with deformation of it. The appropriate boundary conditions can be expressed in terms of total stress, displacements, pore pressures, and flows. However, these boundary conditions must be integrated with the appropriate boundary conditions for the fluid flow model in the fracture. Figure 3 illustrates the relationship between the interface elements and the control volumes for fluid flow in the fracture. There is a one-to-one correspondence between the control volumes and corner nodes



$$-q_{i-1/2}^{n+1} + q_{i+1/2}^{n+1} + \frac{w_i^{n+1} - w_i^n}{\Delta t} \Delta x = -q_{ii}^{n+1}$$

$$-q_{i+1/2}^{n+1} = -\frac{p_{i+1} - p_i}{\Delta x} \frac{\left(\frac{w_{i+1} + w_i}{2}\right)^3}{12\mu}$$

Figure 2. A schematic illustration of the control-volume approach used in the modelling of fluid flow along the fracture

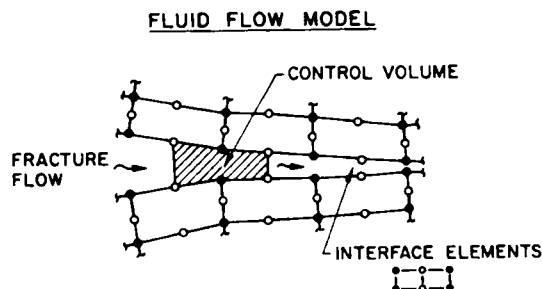


Figure 3. An illustration of a control volume integrated within a finite element mesh

of the finite element mesh along the fracture path. This ensures that fluid mass is conserved across the boundary.

In the examples that follow two methods for coupling can occur along the fracture depending on whether the fracture walls are assumed permeable or impermeable. For impermeable walls, the fluid pressures in the fracture are converted to equivalent nodal loads and applied appropriately. For permeable walls, the fluid pressure in the fracture must be applied as a pore pressure and a total stress boundary condition. It is also necessary to find a solution where the fluid loss from the fracture is consistent with the flow across the boundary of the finite element mesh. This mixed or Cauchy boundary condition for the pressure and flow must be considered in the solution strategy as discussed in the following section.

SOLUTION STRATEGY

In devising a solution strategy for the coupled equations one must weigh several considerations such as computational limitations, future computational capabilities, modularity, robustness of the procedure, reliability and accuracy. The strategy described herein was designed with the prime intent being to create a flexible and robust tool for investigating fracture propagation. It is assumed that there will continue to be large increases in available compute cycles and further development of parallel processing capabilities. These objectives lead to the adoption of a partitioned analysis procedure.

At the heart of the solver is an iteration loop for each time step which is illustrated by a flow chart in Figure 4. The basic procedure involves (1) entering the iteration loop with estimates for u^{t+1} , w^{t+1} and q_f^{t+1} , (2) solving the equation for flow along the fracture for a new estimate of p_f^{t+1} , (where the subscript f is used to indicate only the values along the fracture), (3) estimating the equivalent flow ($q_f^{t+1} = q_i^{t+1}$) to be applied to the finite element mesh boundary, based on the new estimate of p_f^{t+1} and the current estimate for the remaining p^{t+1} , (4) applying the flow boundary conditions and solving the flow equation for the new estimate of the pore pressure field, p^{t+1} , (5) solving the stiffness equation for a new estimate of u^{t+1} and w^{t+1} and, finally, (6) updating the estimate of q_f^{t+1} before returning to (2) if the procedure has not converged.

This method is an iterative procedure that, when using the methods described below, required up to several thousand iterations at each time step before converging to a suitable tolerance. Each iteration consists primarily of a series of vector-matrix multiplications so that it is considerably less expensive than if a matrix inversion was required. Considerable effort was directed initially towards the development of an explicit, staggered solution procedure which would avoid the necessity for iterating at each time step. However, such procedures were found to develop

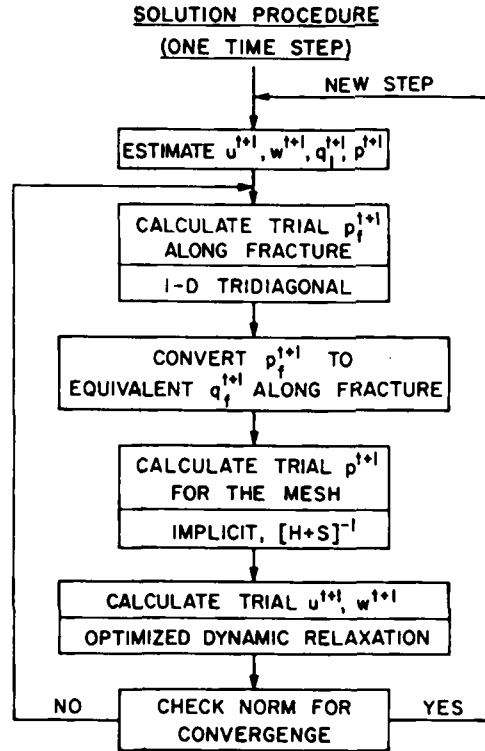


Figure 4. A flow chart of the solution procedure for one time step

numerical oscillations that limited resolution of displacements and pressures in the crack-tip region.

Each of the procedures shown in Figure 4 represents a module of code which can be replaced or modified as the physics of the problem might require. The following observations guided the selection of the particular methods employed here:

1. Implicit-explicit or explicit-implicit solvers have been shown to work well with the finite-element approximation to the theory of poroelasticity.³²
2. Dynamic relaxation (DR) has been found to be a robust method for solving problems with strain-softening materials.³³
3. Implicit formulations that result in tridiagonal matrices are an efficient means for solving one-dimensional fluid flow problems.³⁴
4. Vector operations can be performed efficiently on the hardware available to the authors and it appears to be an increasingly common feature in processors for scientific computing.

In the following sections the specific modules will be described in more detail.

Solution of the finite element equations

The finite element equations were approximated using second-order, finite-difference operators for the time-derivatives as follows:

$$[\mathbf{K}]\{\mathbf{u}^{t+1}\} + [\mathbf{L}]\{\mathbf{p}^{t+1}\} = \{\mathbf{f}^{t+1}\} \quad (15)$$

$$[S] \frac{\{3\mathbf{p}^{t+1} - 4\mathbf{p}^t + \mathbf{p}^{t-1}\}}{2\Delta t} + [L]^T \frac{\{3\mathbf{u}^{t+1} - 4\mathbf{u}^t + \mathbf{u}^{t-1}\}}{2\Delta t} + [H] \{\mathbf{p}^{t+1}\} = \{\mathbf{q}^{t+1}\} \quad (16)$$

Simon *et al.*³² have found that an efficient procedure for the solution of these equations is an explicit-implicit staggered approach. However, they had included dynamic terms which introduced time derivatives in the stiffness equation. By solving equation (15) using DR, an explicit approach, several objectives are attained. First, a pseudo-time is introduced in the stiffness equation facilitating an explicit-implicit, staggered procedure similar to that of Simon. Secondly, the method can be applied to strain-softening, constitutive models for fracture of the rock. Finally, it allows incorporation of a wide range of non-linear constitutive models for the continuum.

DR is also a relatively efficient approach when using a machine with array processing capabilities and is readily adapted to parallel architectures as discussed by Taylor and Flanagan.³⁵ There are several methods for optimizing dynamic-relaxation, as well.³⁶

It is preferable to operate implicitly on the flow equation since the $[H]$ matrix has, typically, a sixth of the row and column dimensions of the $[K]$ matrix. The resulting efficiency is another reason for using a linear approximation to the pore pressure across elements. Since the solution of equation (16) is repeated frequently, it is preferable actually to invert the matrix $[H + S/2\Delta t]$. Although in the past one considered matrix inversion an expensive procedure, with the advent of specialized hardware, such as array processors, the relative cost of inversion has been greatly reduced. In fact, the inversion of the matrix is typically a small fraction of the total computational time.

The Lees operator³⁷ has also been used to replace equation (16) as has been done for the heat equation³⁸:

$$[S] \frac{\{\mathbf{p}^{t+1} - \mathbf{p}^{t-1}\}}{2\Delta t} + [L]^T \frac{\{\mathbf{u}^{t+1} - \mathbf{u}^{t-1}\}}{2\Delta t} + [H] \frac{\{\mathbf{u}^{t+1} + \mathbf{u}^t + \mathbf{u}^{t-1}\}}{3} = \{\mathbf{q}^{t+1}\} \quad (17)$$

The advantage of equation (17) is that it can be used to incorporate non-linear models, such as stress-dependent permeability, in an efficient manner since the matrices are evaluated at the current time step (t) whereas the matrices in equation (16) should be evaluated at the time step ($t + 1$). It is also a second-order approximation. Equation (16) is the preferred form in the absence of non-linearities since equation (17) was observed to cause some minor, time-dependent oscillations in the solution. In either case, the solution of the equation is implicit.

Solution of the fracture flow equations

As mentioned previously, the assembled finite difference approximations produce a tridiagonal matrix. There is little computational efficiency obtained by employing explicit methods in the place of an implicit method that results in a tridiagonal matrix.³⁴ It is therefore preferable to employ an implicit procedure because of the improved stability characteristics. The approximation in equations (13) and (14) is second-order accurate in the space dimension, if Δx is a constant, and first-order accurate in time.

The initial estimates of w^{t+1} , which typically have large relative errors near the crack tip, can result in pressures that have unrealistic magnitudes. It was found that limits must be placed on the acceptable values of p_t^{t+1} in order to prevent these errors from carrying over to the other solution modules. For example, it is reasonable to assume for a propagating fracture that the pressures along the fracture cannot exceed the pressure at the crack-mouth. Nilson has made similar assumptions in order to find solutions for problems of gas flow in fractures.³⁹ At the crack tip, the solver may predict large and unrealistic negative fluid pressures. A limiting minimum pressure

might physically correspond to the apparent vapour pressure of the fluid in the fracture.⁴⁰ Imposing a minimum pressure can identify a void at the crack tip. This is a region where there is insufficient flow from the rock mass or along the fracture to fill it. The presence of this void induces a small error in the current approach. However, since this volume is typically small compared to the volume of the fracture, the error is found to be negligible.

Another mechanism which was found to improve the rate of convergence was the introduction of a term in equation (13) which approximately accounts for changes in q_l between steps of the iteration procedure:

$$-q_{i-1/2}^{t+1} + q_{i+1/2}^{t+1} + \frac{w_i^{t+1} - w_i^t}{\Delta t} \Delta x - q_{ii}^{t+1} - C_i P_i^* = 0, \quad C_i = \left\{ \frac{dq_l}{dP} \right\}_i \quad (18)$$

where P^* is the difference in pressure between the new and current estimates for P^{t+1} along the fracture, and C_i is a geometric parameter that relates a change in fluid loss to the change in pressure. This additional term accounts for the fact that an increase in the fluid pressure in the fracture will increase the leak-off rate. Appropriate coefficients can be determined from the flow matrices in the finite element formulation. The term effectively dampens the pressure changes between iterations and vanishes as the approximation converges.

As mentioned previously, it would be desirable to be able to impose a flow rate at the crack-mouth. This boundary condition is especially useful for verifying the code against known solutions. However, the imposition of a Neuman boundary condition on the crack-mouth pressure (CMP) results in an ill-posed set of equations, within the framework of this solution procedure. Alternatively, the method used has been to estimate p^{t+1} for the CMP, and iterate until an acceptable approximation to the flow rate is achieved. Generally, in a reasonably steady-state flow condition, three iterations are required to find a solution within 1 per cent of the applied flow rate. This increases the required computer time threefold; however, it can be expected that imposition of a Neuman boundary condition would also increase the computational time³⁴ and possibly at the expense of a more limited range for stability and convergence.

Convergence criterion

The norm that has been chosen as a convergence criterion is the sum of the magnitudes of the unbalanced force vector from the DR solution module for the stiffness equation. Since the fluid pressures in the rock mass and along the fracture are represented as force terms in the stiffness equation, the norm is a representative measure of the overall convergence. The value of the norm is problem-dependent. However, an unacceptable convergence criterion produces a distinctive, cyclic variation of the response values about the apparent correct solution.

Adaptive solution control

The solution procedure as implemented has several adaptive solution control features. A variable-time-step option allows the time step to be altered during the process of an analysis. The procedure checks for divergence of the convergence norm and takes appropriate action. For example, when simulating fracture initiation from a borehole, the pressure is typically ramped or increased until a fracture initiates. If the maximum flow rate is limited there will then be an abrupt drop in the fluid pressure at the borehole. The initial estimate of the pressure just after the initiation of the fracture is likely to be excessively high and the solution algorithm may fail to converge. It is appropriate then to reduce the estimate of the pressure and attempt to advance the solution with the revised boundary condition.

It has also been observed, when attempting to solve problems with a limited flow rate at the crack mouth, that at early times, the numerical approximation often does not admit a solution for all flow rates. In fact, the solution range appears to contain a bifurcation consisting of a large jump in the flow rate for a specific CMP. The solution procedure must be capable of recognizing this situation and choosing a solution on one or the other side of the bifurcation; typically the lower flow rate is chosen.

There are both physical and numerical reasons for the existence of such bifurcations; however, it is apparent that solutions do not necessarily exist for all conditions, nor are they necessarily unique when they do exist. For this reason it is important that there be development in the area of adaptive control of coupled problems. If there is not a unique solution to a problem, then it is necessary to be able to direct the solution algorithm to search for a solution within a limited regime, as was discussed previously with regard to flow along the fracture. Partitioned solution procedures are particularly well suited for the incorporation of adaptive control modules in the computer code since they can be interspaced between any or each of the solution modules in the code.

VERIFICATION OF THE NUMERICAL PROCEDURE

Coupled solution procedures are difficult to verify because very few analytical solutions exist for coupled problems. Typically, only selected components of the code can be verified against available solutions. For the case at hand the coupled poroelastic routines are verified against a one-dimensional solution for a column.²⁶ The coupling between fluid flow in a fracture and the finite element approximation is verified for a case where the fracture has impermeable walls.⁴¹ To the best knowledge of the authors, the fully coupled model cannot be compared directly to any known analytical or numerical solutions.

One-dimensional solution for a poroelastic column

The problem of a poroelastic column is given by Detouray, McLennan and Roegiers.²⁶ It is appropriate for verification of the code because it incorporates finite boundaries. The boundary conditions for this problem are given in Figure 5 and the material properties in Table I. Initially, an instantaneous pressure, P , is applied at the top of the column, as both a pore pressure and total stress. It results in a displacement, at the top of the column of

$$u^{0+} = \frac{1 - 2\nu_u}{1 - \nu_u} \frac{PL}{2G} \quad (19)$$

The top of the column rebounds with time resulting in a final deflection, at infinite time, of

$$u^\infty = (1 - \alpha) \frac{1 - 2\nu}{1 - \nu} \frac{PL}{2G} \quad (20)$$

At time 0^+ the pore pressure throughout the column, except at the top boundary, is given by

$$p^{0+} = \frac{B(1 + \nu_u)}{3(1 - \nu_u)} P \quad (21)$$

The initial instantaneous pressure can be used to verify that the coupling in equation (16) is correct. In many cases, typically for time periods $\tau > 1$, the coupling term in this equation is insignificant. Figure 6(a) plots the variation of the fluid pressure at the bottom of the column and

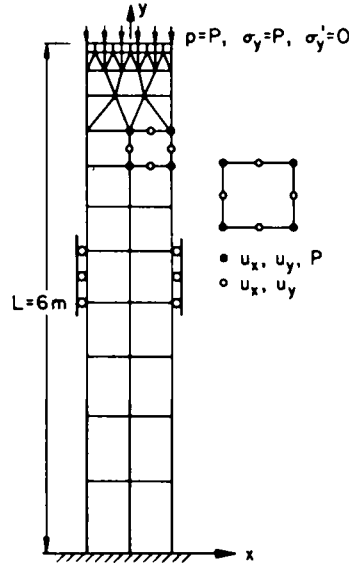


Figure 5. The finite element mesh, dimensions and boundary conditions for the simulation of a one-dimensional column

Table I. Material properties for a water-saturated sandstone⁹

Permeability coefficient	κ	$2 \times 10^{-5} \text{ m}^2/(\text{MPa s})$
Shear modulus	G	6000 MPa
Drained Poisson's ratio	ν	0.2
Undrained Poisson's ratio	ν_u	0.33
Skempton's coefficient	B	0.62
Bulk modulus, solid	K_s	36000 MPa
Bulk modulus, fluid	K_f	3000 MPa
Porosity	η	0.19
Fluid viscosity	μ	10^{-9} MPa s
(both in the rock mass and the fracture)		

Figure 6(b) the variation of the displacement at the top of the column, as a function of time for the analytical solution and the numerical approximation.

Hydraulically driven fracture in an impermeable medium

The concept of a hydraulically-driven, equilibrium fracture has been discussed in detail by Geertsma and Haafkens.⁴² Geertsma and De Klerk had previously derived an approximate solution for the case of a fracture driven by a constant flow rate.⁴³ A more accurate solution to the problem has been published by Spence *et al.*^{41,44} where the solution has been applied to magma flow from the Earth's mantle into long, narrow dykes. The results of both cases can be expressed in the following manner:

$$L = A \left(\frac{GQ^3}{\mu(1-\nu)} \right)^{1/6} t^{2/3} \quad (22)$$

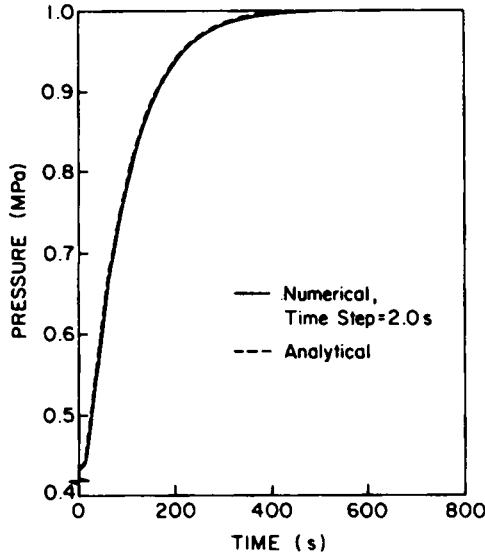


Figure 6(a). A plot of pressure versus time at the base of the column shown in Figure 5

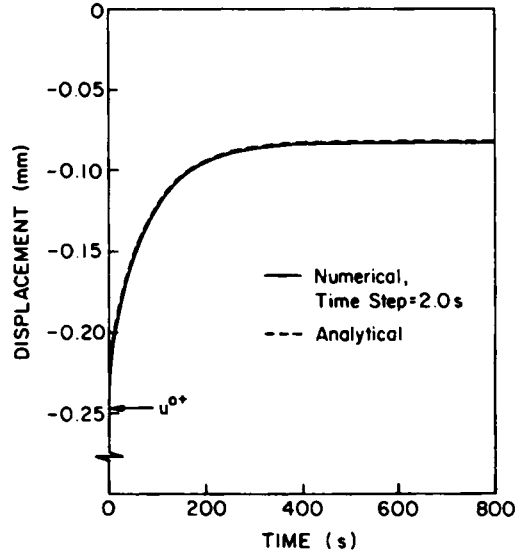


Figure 6(b). A plot of displacement versus time at the top of the column shown in Figure 5.

$$\text{CMOD} = B \left(\frac{\mu(1-\nu)Q^3}{G} \right)^{1/6} t^{1/3} \quad (23)$$

$$P_{\text{cm}} = C \left(\frac{G^3 Q \mu}{(1-\nu)^3 L^2} \right)^{1/4} + S \quad (24)$$

where L is the crack length, Q the flow rate at the crack mouth, t is time, CMOD is the crack-mouth opening displacement, P_{cm} is the pressure at the crack-mouth and S is the *in situ* stress normal to the crack path. A , B and C are constants, which are Spence's solution are 0.65, 2.14 and 1.97, respectively. The corresponding values given by Geertsma and Haafkens⁴² are 0.68, 1.87 and 1.38.

The finite element mesh shown in Figure 7 has been used to approximate the boundary conditions for the case described by Spence and Geertsma. A constant flow rate of 0.0001 m³/s was applied at the fracture mouth, assuming a single-sided fracture. In Figure 8 the length, CMOD and pressure at the crack-mouth are plotted against time, verifying that the results of the finite element analysis closely match the Spence *et al.* solution.

Comparisons are also made with the pressure distribution and crack opening displacement in Figure 9. It is apparent that there is a discrepancy between the numerical results and Spence's solution near the crack-tip. This can be attributed to an imposed minimum pressure of zero in the numerical solution, whereas there is no imposed minimum in Spence's solution. As discussed previously, there is evidence that, in theory, the pressure at the crack-tip is singular.³¹ Physically this is interpreted as suggesting there must be a lag between the fracturing fluid and the crack-tip. However, the lag apparently cannot be resolved by the mesh refinement used in this example problem. Over the rest of the crack length the results agree well.

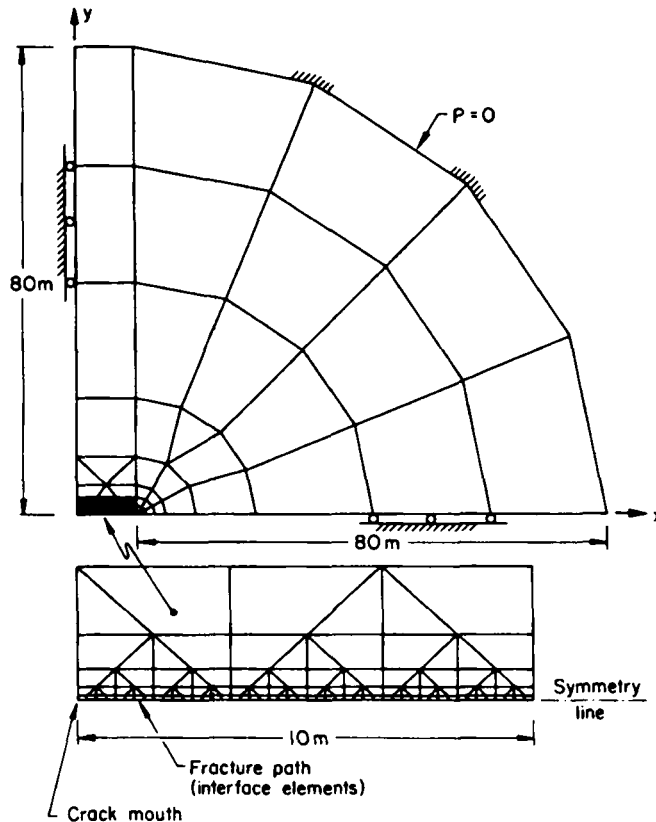


Figure 7. The finite element mesh used for simulating the propagation of hydraulically-driven fractures

Fully coupled, propagating fracture

In the final example, results of a fully-coupled, propagating fracture are presented. The finite element mesh is the same as that shown in Figure 7 with the material properties given in Table I. A constant flow rate of $0.0005 \text{ m}^3/\text{s}$ was applied at the crack-mouth. Plots of the crack length, CMOD and CMP versus time are shown in Figure 10. A plot of the fracture volume and the total volume of fluid pumped into the fracture are shown in Figure 11 as a function of time.

The plots in Figures 10 and 11 provide useful information about the fracture growth, but they provide little information about coupling throughout the domain. Clearly, there is much more information contained in the numerical results. In order to explore better the results of the analysis a graphics display tool, or program, which runs on a high performance engineering workstation has been developed.⁴⁵ It allows the user to select a variety of response parameters and to plot the values in relief and/or using colour contouring. The images can be displayed as a sequence which produces an animated effect and allows one to correlate various response characteristics in time and space.

Plate 1 shows a series of photographs for this example problem taken at a time of 9.6 s. In Plate 1(a) the finite element mesh, from Figure 7 is shown in a three-dimensional perspective. The menu from the interactive computer code for displaying the simulated results is shown in the top right corner, and a bar code for colour contouring is shown on the right-hand side. For pedagogical

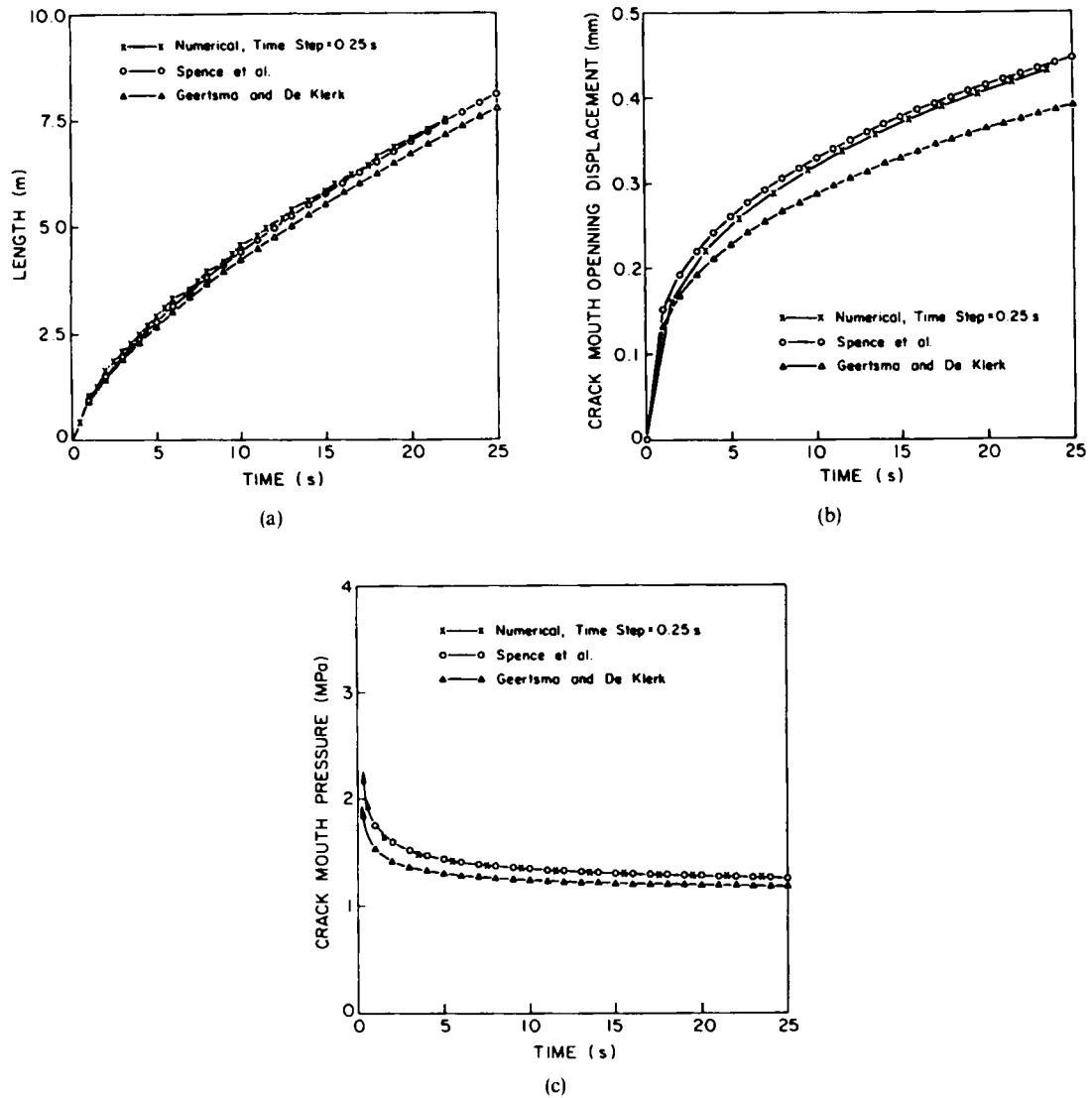


Figure 8. Comparison of results for a hydraulically-driven fracture in an impermeable medium attained from (i) the procedure described herein, (ii) Geertsma and De Klerk's solution^{4,3} and (iii) Spence *et al.*'s solution.^{4,1} Plots are of (a) crack length versus time, (b) crack-mouth-opening displacement versus time and (c) crack-mouth pressure versus time

purposes the program reflects the results of the quarter-symmetric analysis and shows a complete double-sided fracture. In Plate 1(b) the pore-pressure distribution is plotted in relief, and stress, σ'_x , is displayed using colour contours. The resulting surface plot is shown relative to the deformed, finite element mesh so that the crack-opening profile is clearly visible. In Plate 1(c) the figure has been rotated so that the crack-opening profile is visible and one can see the smoothly closing crack-tip which is distinctive characteristic of the Dugdale-Barenblatt model. A second distinctive feature is the depression in the pore pressure ahead of the crack-tip. This effect is present in Ruina's solution^{1,2} and is indicative of an apparent increase in the fracture toughness that he predicts using

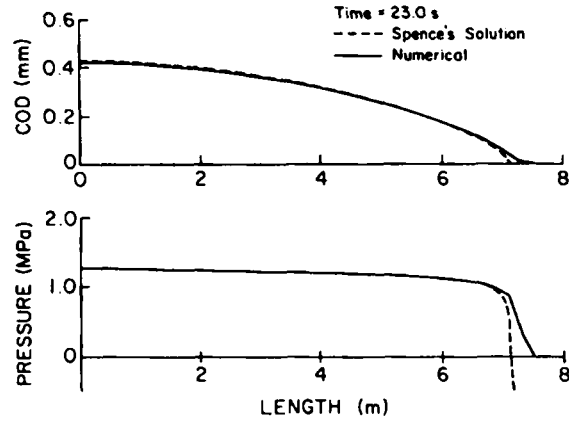


Figure 9. Plots of crack-opening displacement and pressure along the crack length at 23.0 s, for the procedure presented herein and Spence *et al.*'s solution.⁴¹

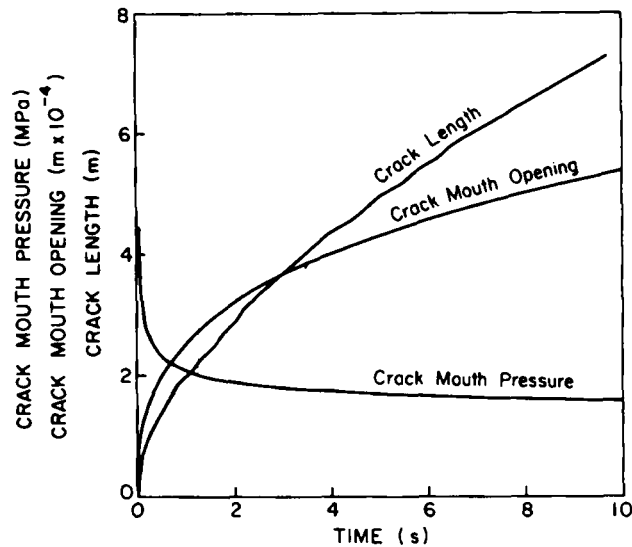


Figure 10. Plots of crack length, crack-mouth opening, and crack-mouth pressure versus time for a fully-coupled simulation of a hydraulically-driven fracture in a permeable rock mass

an effective stress as a failure criterion. A scaled, vertical cutting plane has been introduced in Plate 1(d) to quantify better the pore pressure values. In Plate 1(e), the total stress, σ_y , is now plotted in relief contrasting σ'_y , which is plotted using colour contours. Here it is seen that σ'_y is zero along the crack walls, which is the appropriate boundary condition, and accordingly the magnitude of σ_y is equal to the pore pressure. The finite element mesh is located in the plane $\sigma_y = 0$. Finally, in Plate 1(f) p is shown in relief and the principle directions of fluid flow are depicted by arrows superposed on the relief plot. A characteristic flow pattern from the region in the close vicinity of the crack faces into the region ahead of the crack-tip was observed throughout the simulation.

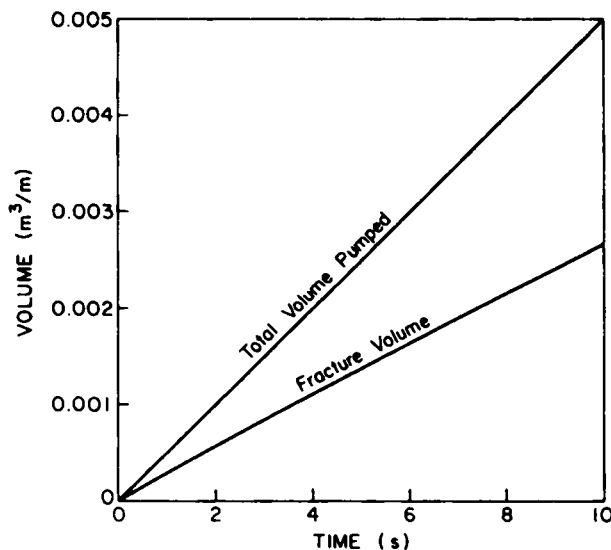


Figure 11. A plot of the fracture volume and the total volume of fluid pumped for the fully-coupled simulation

The authors have found this display tool to be extremely useful. It provides (1) rapid display of large quantities of numerical data in a comprehensible form, (2) insight into the nature of the physically coupled processes, (3) rapid verification of the applied boundary conditions, (4) insight into the quality of the numerical analysis and (5) a useful and powerful tool for assisting in code development.

DISCUSSION AND CONCLUSIONS

The proposed solution algorithm attains much of its robustness from the use of a DR scheme for solution of the stiffness equation. This characteristic is especially important when considering fracture mechanics problems. Problems involving fracture often have instabilities associated with sudden extensions in the fracture length and the release of strain energy. Models for tensile failure of rock incorporate strain-softening, which poses similar problems. For hydraulically driven fractures, these effects are particularly important when attempting to model fracture initiation, and break-down for a pressurized borehole. All these considerations lead to the conclusion that a robust and 'forgiving' solver for the stiffness equations is extremely important. The solver should also allow one to determine readily if the solution is diverging so that adaptive control modules in the code can take corrective action.

The example problems raise several points worthy of discussion. The first example illustrates that there can be very significant time-dependent changes in the deformation of a structure due to poroelastic effects. The second shows that the model presented herein is in good agreement with the work of Spence *et al.*⁴¹ which predicts higher pressures at the borehole than the Geertsma-De Klerk model.⁴²

There is experimental evidence that the tip of a crack in rock closes smoothly, as in the Dugdale-Barenblatt model, and that there is a lag between the fluid front and the crack tip.^{46,47} The experimentally observed fluid lag was in fractures of several centimeters in length and found to represent as much as 10–20 per cent of the crack length. A fluid lag was not observed in the numerical approximations presented herein. But clearly, a lag of only a few centimetres could not be resolved by the mesh that was used. However, the results do suggest that in the presence of even

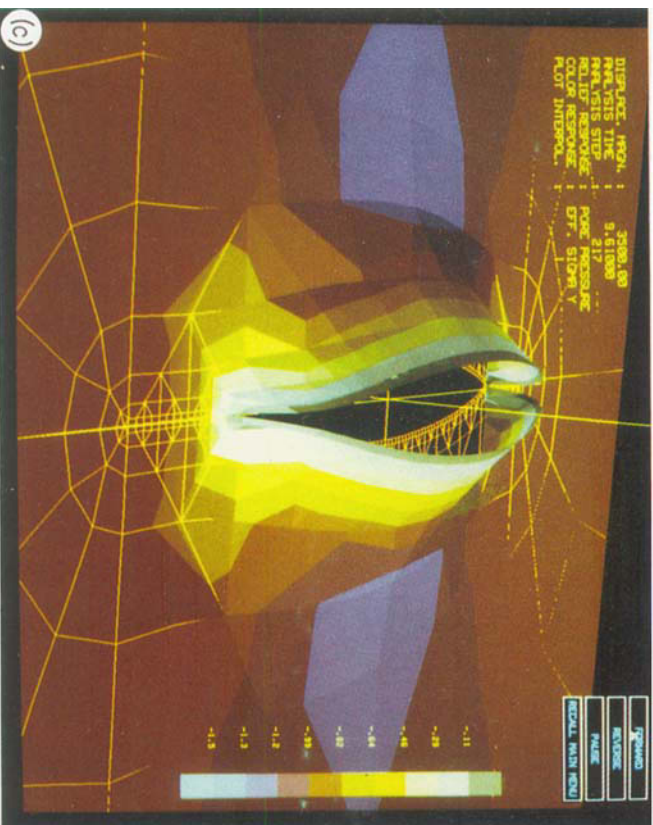
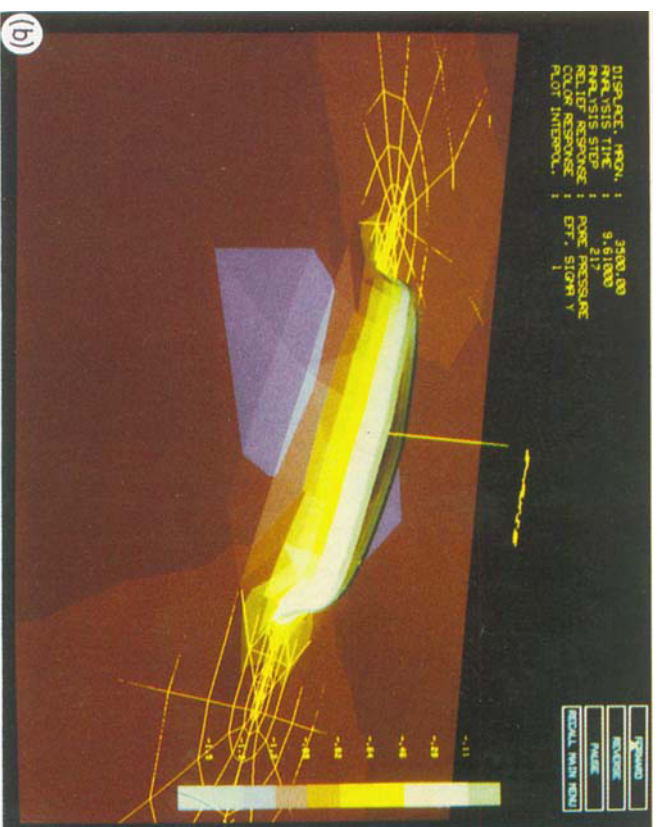
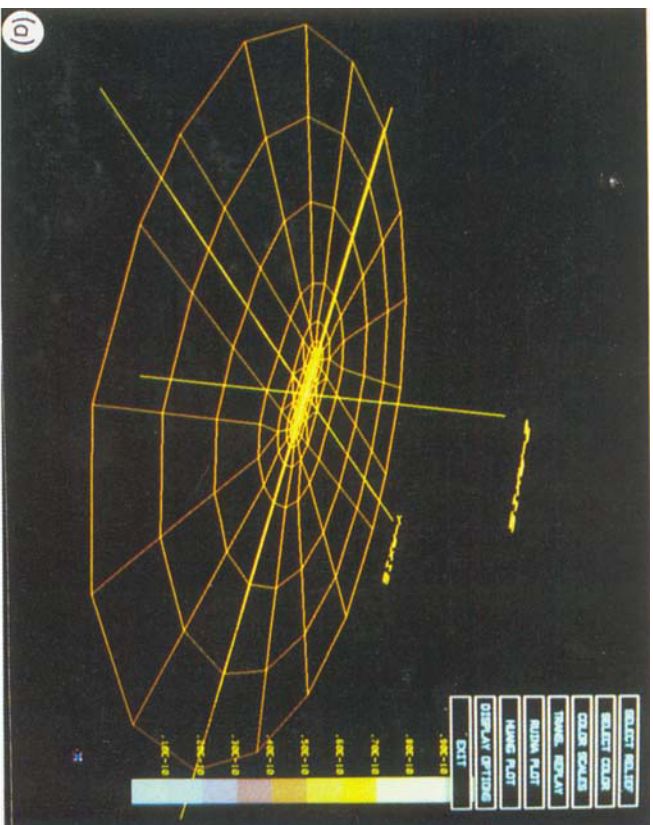


Plate 1. A series of photographs taken from a high-performance engineering workstation at a time of 9.6s, which illustrate (a) the finite element mesh from Figure 7 positioned in three-dimensional plot space; (b), (c) various plots with effective stress σ_e , represented by colour contours and pore pressure, p , plotted in relief

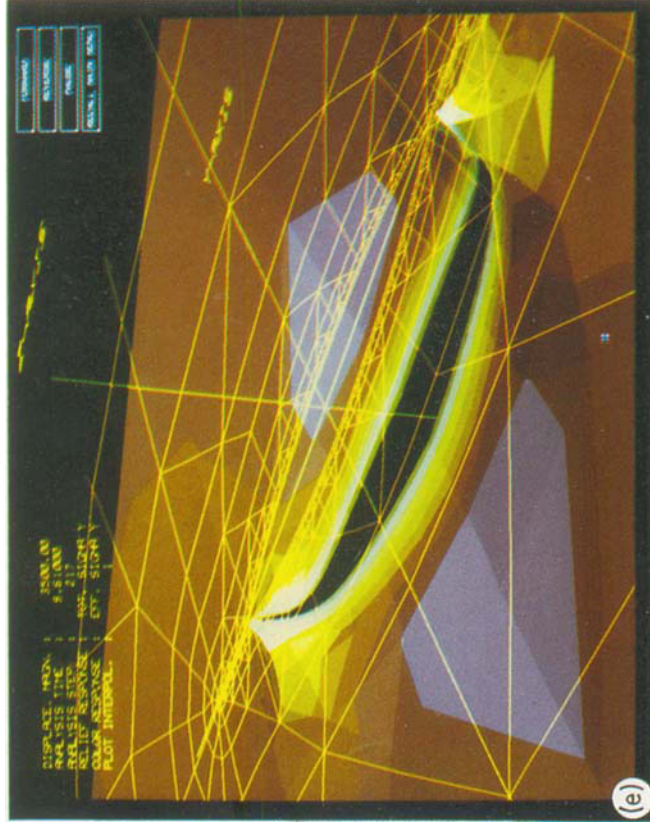
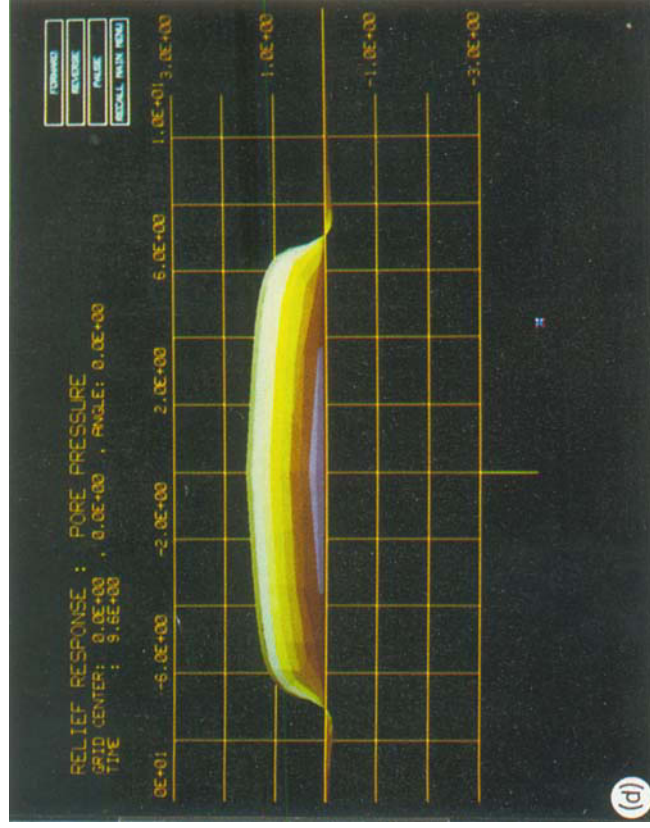


Plate 1. (d) Further plots with effective stress σ'_y , represented by colour contours and pore pressure, p , plotted in relief; (e) total stress, σ_y , in relief and effective stress σ'_y , represented by colour contours; and (f) pore pressure, p , in relief with the arrows, representing the direction of flow, superposed

moderate *in situ* compressive stress normal to the fracture, there is not likely to be a significant fluid lag behind the crack-tip at the scales of typical hydraulic fractures in the field. The fluid lag is not expected to scale linearly with the crack length, given a constant flow rate at the crack mouth. Factors outside the scope of this investigation, which could potentially produce a significant fluid lag, are high flow rates or very viscous fluids.

One of the purposes for developing a fully-coupled model for hydraulically driven fracture propagation is that currently, largely one-dimensional, empirical relationships are used to calculate expected fluid losses in the field.⁴⁸ A more advanced multidimensional model could be developed on the basis of poroelastic analyses. It is therefore interesting to note that there is a near constant relationship exhibited between the total volume of fluid flow and the fracture volume, as shown in Figure 11. This simple, low-order relationship starkly contrasts with the two-dimensional, flow pattern as shown in Plate 1(f). The direction of flow is predominantly from the fracture towards the region of high volumetric strain ahead of the crack-tip.

It was assumed in the final example that the fluid that leaked off from the fracture had the same characteristics as the fluid saturating the rock. In reality there may be very large differences. Practically, this is accounted for through concepts such as 'filter-cake' and 'spurt-loss'.⁴⁸ In a poroelastic model it might be appropriate to model the advance of the fluid interface between the fluid lost from the fracture and the fluid which initially saturated the rock mass. This model could replace the empirical concepts just cited.

As noted in the introduction, it is expected that poroelastic effects in conjunction with an effective stress criterion could produce an increase in the apparent fracture toughness (K_Q) of rock. The proposed procedure could be used to quantify the effects by incorporating a strain softening model for the fracture process zone, as has been discussed by Cleary^{10,11} and illustrated in Reference 49.

Extending the procedure to three-dimensions should be a straightforward process. Some advantages are that the DR solver for the stiffness equations is relatively more efficient for larger problems, the dimension of the $[H]$ relative to the $[K]$ matrix reduces to 1:8 from 1:6, and the method for finding the fracture dimensions is inherent in the procedure. One disadvantage is that a two-dimensional model for fluid flow in the fracture cannot use a tridiagonal solver, and will therefore be a more significant computational expense.

The numerical procedure described in this paper has been shown to be reasonably successful. However, work must still be done to improve the efficiency of the algorithm, to determine appropriate conditions for stability and to verify general convergence in the time and space domains.

ACKNOWLEDGEMENTS

This work has been sponsored in part by a grant from the U.S. National Science Foundation, No. PYI 8351914. Corporate sponsorship by Dowell-Schlumberger, Digital Equipment Corporation and the Hewlett-Packard Company is gratefully acknowledged. The research was conducted at the Program for Computer Graphics, Cornell University. The advice of Dr. Emmanuel Detournay and Dr. Jean-Claude Roegiers has also been greatly appreciated.

APPENDIX: FORMULATION OF THE FINITE ELEMENT MATRICES

Let $p = N^p\{\mathbf{p}\}$, $u = N^u\{\mathbf{u}\}$ and $\varepsilon = \mathbf{B}\{\mathbf{u}\}$ where N^p and N^u are the nodal shape functions for pressure and displacements, respectively.

$$[\mathbf{K}] = \int_{\Omega} \mathbf{B}^T \mathbf{D} \mathbf{B} d\Omega \quad (25)$$

where \mathbf{D} is the drained, material elasticity matrix.¹⁹

$$[\mathbf{L}] = \alpha \int_{\Omega} \mathbf{N}^u \left\{ \frac{\delta}{\delta x} \right\} \mathbf{N}^p d\Omega \quad (26)$$

$$[\mathbf{H}] = \kappa \int_{\Omega} \left\{ \frac{\delta}{\delta x} \right\} \mathbf{N}^p \left\{ \frac{\delta}{\delta y} \right\} \mathbf{N}^p d\Omega \quad (27)$$

$$[\mathbf{S}] = \int_{\Omega} \mathbf{N}^p \frac{1}{Q} \mathbf{N}^p d\Omega \quad (28)$$

$$\frac{1}{Q} = \left(\frac{\phi}{K_f} + \frac{1-\phi}{K_s} - \frac{1-\alpha}{K_s} \right) = \frac{\alpha(1-\alpha B)}{BK} = \frac{9(v_u - v)(1 - 2v_u)}{2GB^2\kappa(1 - 2v)(1 + v_u)^2} \quad (29)$$

REFERENCES

1. D. A. Mendelsohn, 'A review of hydraulic fracture modeling—I: general concepts, 2D models, motivation for 3D modeling', *J. Energy Resources Tech.* **106**, 369–376 (1984).
2. D. A. Mendelsohn, 'A review of hydraulic fracture modelling—II: 3D modeling and vertical growth in layered rock', *J. Energy Resources Tech.*, **106**, 543–553 (1984).
3. G. R. Olhoft, *Annual Review of U.S. Progress in Rock Mechanics—Coupled Processes*, National Academy Press, Washington, D.C., 1987.
4. K. C. Park and C. A. Filippa, 'Partitioned analysis of coupled systems', in T. Belytschko and T. J. R. Hughes (eds), *Computational Methods for Transient Response Analysis*, North-Holland, 1982, pp. 157–219.
5. K. C. Park and C. A. Filippa, 'Recent developments in coupled field analysis methods', in R. W. Lewis, P. Bettess and E. Hinton (eds) *Numerical Methods in Coupled Systems*, Wiley, Chichester, 1984, pp. 327–351.
6. O. C. Zienkiewicz, 'Coupled problems and their numerical solution', in R. W. Lewis, P. Bettess and E. Hinton (eds), *Numerical Methods in Coupled Systems*, Wiley, Chichester, 1984, pp. 35–58.
7. M. A. Biot, 'General theory of three-dimensional consolidation', *J. Appl. Phys.*, **12**, 155–164 (1941).
8. M. A. Biot, 'General solutions of the equations of elasticity and consolidation for a porous material', *J. Appl. Mech.*, **23**, 91–96 (1956).
9. J. R. Rice and M. P. Cleary, 'Some basic stress diffusion solutions for fluid-saturated elastic porous media with compressible constituents', *Rev. Geophys. and Space Phys.*, **14**, 227–241 (1976).
10. M. P. Cleary, 'Fundamental solutions for fluid-saturated porous media and application to localized rupture phenomena', *Ph.D. Dissertation*, Brown University, Providence, RI, 1976.
11. M. P. Cleary, 'Rate and structure sensitivity in hydraulic fracturing of fluid-saturated porous formations', in K. Gray (ed.), *Proc. 20th U.S. Rock Mechanics Symposium*, Austin, TX, 1979.
12. A. Ruina, 'Influence of coupled deformation-diffusion effects on the retardation of hydraulic fracture', *Proc. 19th U.S. Rock Mechanics Symposium*, 1978, pp. 274–282.
13. N. C. Huang and S. G. Russell, 'Hydraulic fracturing of a saturated porous medium—I: general theory', *Theoret. Appl. Fracture Mech.*, **4**, 201–213 (1985).
14. N. C. Huang and S. G. Russell, 'Hydraulic fracturing of a saturated porous medium—II: special cases', *Theoret. Appl. Fracture Mech.*, **4**, 215–222 (1985).
15. A. R. Ingraffea and T. J. Boone, 'Simulation of fracture propagation in poroelastic rock', in G. Swoboda (ed.), *Numerical Methods in Geomechanics—Innsbruck 1988*, Rotterdam, 1988, pp. 95–105.
16. E. Detournay and A. H.-D. Cheng, 'Poroelastic response of a borehole in a non-hydrostatic stress field', *Int. J. Rock Mech. and Mining Sci.*, **25**, (3), 171–182 (1988).
17. J. R. Rice, 'Pore pressure effects in inelastic constitutive formulations for fissured rock masses', *Advances in Civil Engineering through Engineering Mechanics*, ASCE, New York, 1977.
18. G. K. Batchelor, *An Introduction to Fluid Dynamics*, Cambridge University Press, New York, 1967.
19. O. C. Zienkiewicz, 'Basic formulation of static and dynamic behaviour of soil and other porous media', in J. Martinus (ed.), *Numerical Methods in Geomechanics*, Holland, 1982, pp. 39–56.
20. R. S. Sandhu, H. Liu and K. H. Singh, 'Numerical performance of some finite element schemes for analysis of seepage in porous elastic media', *Int. j. numer. anal. methods geomech.*, **1**, 177–194 (1977).
21. R. E. Goodman, R. L. Taylor and T. L. Brekke, 'A model for the mechanics of jointed rock', *J. Soil Mech. Fdns Div., Am. Soc. Civ. Engrs*, **94**, (5), (SM3), 637–659 (1968).
22. D. Broek, *Elementary Engineering Fracture Mechanics*, 3rd, edn, Martinus Nijhoff, The Hague, 1982.
23. T. J. Boone, P. A. Wawryznek and A. R. Ingraffea, 'Simulation of the fracture processes in rock with application to hydrofracture', *Int. J. Rock Mech. Min. Sci. & Geomech. Abstr.*, 255–265 (1986).

24. M. P. Cleary, 'Analysis of mechanisms and procedures for producing favorable shapes of hydraulic fractures', *SPE* 9260 (1980).
25. M. P. Cleary and S. K. Wong, 'Numerical simulation of unsteady fluid flow and propagation of a circular hydraulic fracture', *Int. j. numer. anal. methods geomech.*, **9**, 1-14 (1985).
26. E. Detouray, J. D. McLennan and J.-C. Roegiers, 'Poroelastic concepts explain some of the hydraulic fracture concepts', *SPE* 15262 (1985).
27. A. H.-D. Cheng and E. Detouray, 'A direct boundary element method for plane strain poroelasticity', submitted to *Int. numer. anal. methods geomech.*, **12**, 551-572 (1988).
28. L. Vandamme, E. Detournay and A. H.-D. Cheng, 'A two-dimensional poroelastic displacement discontinuity method for hydraulic fracture simulation', *Int. j. numer. anal. methods geomech.*, **13**, 215-224 (1988).
29. R. S. Sandhu, S. C. Lee and H.-I. Tee, 'Special finite elements for analysis of soil consolidation', *Int. j. numer. anal. methods geomech.*, **9**, 125-147 (1985).
30. P. Bettess and J. A. Bettess, 'Infinite elements for static problems', *Eng. Comput.*, **1**, 4-16 (1984).
31. H. Abe, T. Mura and L. M. Keer, 'Growth rate of a penny-shaped crack in hydraulic fracturing of rocks', *J. Geophysical Res.*, **81** (29), 5335-5340 (1976).
32. B. R. Simon, J. S.-S. Wu, O. C. Zienkiewicz and D. K. Paul, 'Evaluation of u - w and u - p finite-element methods for the dynamic response of saturated porous media using one-dimensional models', *Int. J. numer. anal. methods geomech.*, **10**(5), 461-482 (1986).
33. P. A. Wawrzynek, T. J. Boone and A. R. Ingraffea, 'Efficient techniques for modelling the fracture process zone in rock and concrete', in A. R. Luxmoore *et al.* (eds), *Proc. 4th Int. Conf. Numerical Methods in Fracture Mechanics*, Swansea, 1987, pp. 473-479.
34. Y. Jaluria and K. E. Torrance, *Computational Heat Transfer*, Hemisphere Publishing Corp., Washington 1986.
35. L. M. Taylor and D. P. Flanagan, 'PRONTO2D, a two-dimensional, transient solid dynamics program', *SAND 86-0594*, Sandia National Laboratories, Albuquerque, NM 1987.
36. P. Underwood, 'Dynamic relaxation---a review', in T. Belytschko and T. J. R. Hughes (eds), *Computational Methods for Transient Response Analysis*, North-Holland, 1983, pp. 245-265.
37. M. Lees, 'A linear three-level difference scheme for quasilinear parabolic equations', *Maths. Comp.*, **20**, 516-522 (1966).
38. G. Comini, S. Del Guidice, R. H. Lewis and O. C. Zienkiewicz, 'Finite element solution of the nonlinear heat conduction problems with special reference to phase change', *Int. J. Numer. Methods Eng.*, **8**, 613-624 (1974).
39. R. H. Nilson, 'An integral method for predicting hydraulic fracture propagation driven by gases or liquids', *Int. j. numer. anal. methods geomech.*, **10**, 191-211 (1986).
40. Y.-C. Fung, *A First Course in Continuum Mechanics*, Prentice-Hall, Inc., Englewood Cliffs, NJ, 1969.
41. D. A. Spence and P. Sharp, 'Self-similar solutions for elastohydrodynamic cavity flow', *Proc., R. Soc. Lond.*, **A 400**, 289-313 (1985).
42. J. Geertsma and R. Haafkens, 'A comparison of the theories for predicting width and extent of vertical hydraulically induced fractures', *J. Energy Resources Tech.*, **101**, 8-19 (1979).
43. J. Geertsma and F. De Klerk, 'A rapid method of predicting width and extent of hydraulically induced fractures', *J. Petroleum Tech.*, **21**, (12), 1571-1581 (1969).
44. S. H. Emmerman, D. L. Turcotte and D. A. Spence, 'Transport of magma and hydrothermal solutions by laminar and turbulent fluid fracture', *Phys. Earth Planetary Interiors*, **41**, 249-259 (1986).
45. T. J. Boone, A. R. Ingraffea and J.-C. Roegiers, 'Visualization of hydraulically-driven fracture propagation in poroelastic media using a super-workstation', Submitted to the SPE, August 1988.
46. A. A. Daneshy, 'Hydraulic fracture propagation in layered formations', *Soc. Pet. Eng. J.*, **18**, 33-41 (1978).
47. W. L. Medlin and L. Masse, 'Laboratory experiments in fracture propagation', *Soc. Pet. Eng. J.*, **24**, 256-268 (1984).
48. V. G. Constien, 'Fracturing fluid and proppant characterization', in M. J. Economides and K. G. Nolte (eds), *Reservoir Stimulation*, Schlumberger Educational Services, 1987.
49. T. J. Boone and A. R. Ingraffea, 'Simulation of fracture propagation in poroelastic materials with application to the measurement of fracture parameters', in H. Mihashi (ed.), *Proc. International Workshop on Fracture Toughness and Fracture Energy—Test Methods for Concrete and Rock.*, Sendai, Japan, 12-14 October 1988.